Urban land cover classification potential of high and very-high resolution SAR imagery

Fabio Pacifici[1], Fabio Del Frate[1], Domenico Solimini[1] and Alessandro Burini [2]

[1] Earth Observation Laboratory, Tor Vergata University, Rome, ITALY (f.pacifici@disp.uniroma2.it)

[2] Geo-K S.r.l. Via del Politecnico, 1 00133 Rome, ITALY (alessandro.burini@geok.it)

ABSTRACT – Remote sensing in the optical band is a well established tool for producing and updating maps of urban land use and monitoring changes, but it can suffer from atmospheric limitations, especially where clouds systematically occurs or when unpredictable abnormally long periods of cloud cover affect usually clear-sky regions. Hence, when a systematic, timely and reliable survey of an urban area is required, the use of SAR imagery might become suitable or even necessary. The aim of this poster is to bound the potential of the ERS data in identifying land cover in large urban areas. In fact, the C-band SAR data provided in the past years by ERS-1 and ERS-2, and currently by ENVISAT, are systematically available at relatively low price. Together with LANDSAT, they provide a decadal history of the urban areas, hence their value should not be neglected, rather it deserves particular attention. Moreover, the ERS image long time series provide a unique reliable means of systematically tracking, retrieving and understanding the frequently dramatic changes undergone by the land cover of large cities in all parts of the world in the past 15 years. Because of the decametric size of the resolution cells at ground, the shapes of the structures are altered and mixed pixels are expected, especially in a sub-urban landscape, where heterogeneous land covers are present over short distances.

DATA SET – The data set was composed by ten ERS SAR images acquired over the city of Rome, Italy, as reported in the following tables.

Site Information			Images Information			
Location	Dimension (km²)	Acquisition Date	Satellite	Spatial Res. (m)	Dimension (pixels)
Rome, Italy	836	January 25, 1994	ERS 1	30	1245 x 1300
		January 31, 1994	ERS 1	30	
		March 26, 1994	ERS 1	30	
		March 29, 1994	ERS 1	30	
		July 13, 1994	ERS 1	30	

Site Information		Images Information			
Location	Dimension (km²)	Acquisition Date	Satellite	Spatial Res. (m)	Dimension (pixels)
Rome, Italy	836	February 13, 1999	ERS 1	30	1245 x 1300
		February 14, 1999	ERS 2	30	
		March 20, 1999	ERS 1	30	
		March 21, 1999	ERS 2	30	
		July 4, 1999	ERS 2	30	

FEATURES SELECTION – To attain a sufficient classification accuracy, careful selection and suitable processing are required to exploit the various pieces of information embedded in both the amplitude and phase of the radar return and in its time-space behaviour.

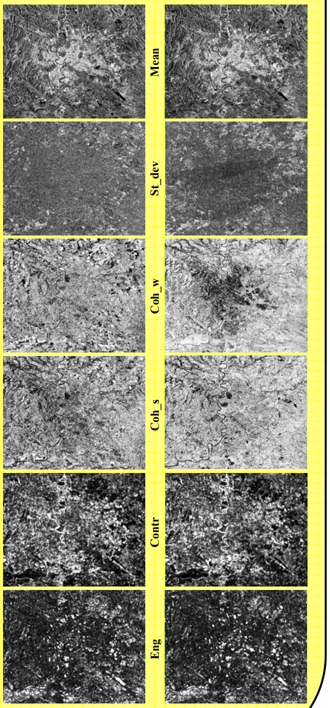

Features affected by different scattering mechanisms and sensitive to the geometry of the scatterers have the potential of maximizing the quantity of information available to the algorithm. To this end, we used two features related to the backscattering mechanisms, two textural features and two features related to the phase information, contained in the ERS-SLC images.

The information contained in the backscattering has been exploited by considering the time-average and the standard deviation values computed over the 5 dates for each year. The textural features consist in the *Contrast* and *Energy*, chosen among the variety of textural parameters. On the basis of several tests aimed at increasing the separability among classes, the features were computed over moving square boxes of 7x7 pixels, and considering a 16 grey levels quantization. Finally, the phase information has been included into two degree of interferometric coherence values, one calculated over two winter tandem acquisitions, the other one over two late spring tandem acquisitions.

	Output Classes	1994 (points)	1999 (points)
1	AS Asphalt	608	731
2	FO Forest	1504	3342
3	HD High Density	707	926
4	IB Isolated Buildings	195	174
5	LD Low Density	4145	7247
6	VE Vegetation	2637	4475
7	WS Water	1067	1274
(8)	FFO Fore Forest	238	363
(9)	FVE Fore Vegetation	594	577
	TOTAL ROIs	11689	19109
	TRAINING ROIs	8182	13376
	VALIDATION ROIs	3507	5733

REGION OF INTEREST SELECTION – Given the peculiarities of the SAR image generation, we decided to include two radar-specific target types into the set of traditional land cover classes. The two fictitious classes are needed because of the acquisition geometry and do not correspond to real surface types, analogously to shadowed areas in optical images. In particular we intended to single out the sloppy hilly areas affected by foreshortening, which appear in different vegetated and forested areas around the city. The classes *fore-forest* (FFO) and *fore-vegetation* (FVE), have thus been added to the commonly used land cover classes: asphalt (AS), water (WA), high-density residential (HD), low-density residential (LD), isolated buildings (IB), arboreous (FO), agricultural areas (VE). In general, the backscattering feature dominates over the urban areas, the coherence feature characterizes the vegetated areas and the texture features are particularly apparent in the zone of the Tiber river bed. In fact, the tables point out that the ambiguity between arboreous and low-vegetation areas can be resolved by the degree of coherence, and the one between low vegetation and low-density residential, by the texture *Contrast*.

Mean of Features – 1994

Feature	AS	FO	HD	IB	LD	VE	WS	FFO	FVE
Mean	-14.056	-8.178	-3.153	3.118	-5.079	-8.909	-16.184	-5.716	-4.468
St_dev	1.820	1.557	1.633	1.910	1.607	1.716	2.239	1.510	1.735
Coh_w	0.521	0.310	0.656	0.729	0.629	0.615	0.318	0.408	0.618
Coh_s	0.510	0.197	0.605	0.689	0.512	0.554	0.246	0.224	0.467
Contr	9.814	7.964	7.080	10.783	7.775	5.331	14.345	13.655	9.026
Eng	0.143	0.034	0.065	0.245	0.035	0.060	0.053	0.027	0.028

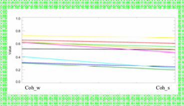

Mean of Features - 1999

Feature	AS	FO	HD	IB	LD	VE	WS	FFO	FVE
Mean	-13.390	-8.401	-3.103	4.641	-4.915	-9.769	-14.654	-8.256	-4.938
St_dev	1.644	1.604	1.376	1.981	1.574	1.993	2.432	1.790	2.230
Coh_w	0.566	0.329	0.440	0.602	0.471	0.654	0.343	0.343	0.473
Coh_s	0.610	0.313	0.754	0.825	0.678	0.650	0.290	0.378	0.698
Contr	8.579	7.771	6.978	11.071	7.437	5.246	14.602	11.182	9.516
Eng	0.128	0.035	0.074	0.306	0.040	0.067	0.047	0.037	0.028

St_dev of Features – 1994

Feature	AS	FO	HD	IB	LD	VE	WS	FFO	FVE
Mean	2.217	2.447	1.594	5.194	1.980	2.122	2.191	2.743	1.861
St_dev	0.647	0.577	0.687	1.200	0.674	0.731	1.198	0.719	0.684
Coh_w	0.147	0.132	0.091	0.174	0.124	0.187	0.131	0.157	0.133
Coh_s	0.130	0.082	0.090	0.136	0.160	0.165	0.104	0.107	0.149
Contr	6.094	4.064	3.925	5.552	2.908	3.555	6.056	5.400	2.309
Eng	0.178	0.011	0.031	0.168	0.009	0.039	0.024	0.006	0.005

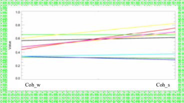

St_dev of Features - 1999

Feature	AS	FO	HD	IB	LD	VE	WS	FFO	FVE
Mean	2.004	2.373	1.874	5.799	2.185	2.096	2.121	3.724	1.881
St_dev	0.709	0.570	0.595	1.253	0.611	0.730	0.915	0.656	0.745
Coh_w	0.111	0.144	0.130	0.136	0.166	0.093	0.139	0.137	0.147
Coh_s	0.134	0.130	0.062	0.058	0.093	0.155	0.121	0.159	0.107
Contr	5.790	3.702	3.828	5.346	3.421	3.594	5.829	5.720	3.313
Eng	0.171	0.011	0.038	0.194	0.020	0.056	0.031	0.020	0.005

NEURAL NETWORK DESIGN – Among various topologies, MultiLayer Perceptrons have been found to have the best suited topology for classification and inversion problems. As far as the numbers of hidden layers and of their units are concerned, the topology providing the optimal performance should be selected on the basis of a suitable compromise. We see that, as expected, increasing the number of hidden neurons is effective up to a given number, after that the SSE value does not change significantly. The results show a good stability (low standard deviation values) with respect to different initializations of the network. At the end, a configuration with two-hidden layers with 60 neurons each was chosen.

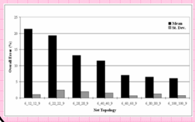

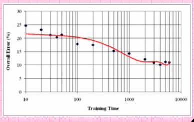

Classification Map of 1994

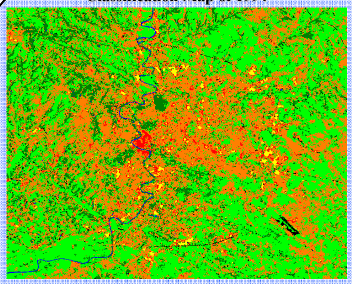

	AS	FO	HD	IB	LD	VE	WS	TOT	Excl Err (%)
AS	165	0	0	0	0	2	0	167	1.2
FO	0	488	0	0	15	15	0	518	5.8
HD	0	1	[illegible]	0	13	0	0	[illegible]	[illegible]
IB	0	0	0	57	2	0	0	59	3.4
LD	4	19	30	2	1175	93	1	1324	11.3
VE	11	10	3	0	40	837	1	902	7.2
WS	2	4	0	0	0	0	318	324	1.9
TOT	182	522	222	59	1245	945	320	3507	
Incl Err (%)	[illegible]								
Overall Error (%)	[illegible]				k-Coefficient	[illegible]			

CLASSIFICATION MAPS – The classification exercise has been carried out for ERS data set acquired in 1994 and 1999, thus obtaining two different land cover maps, whose comparison yields the large-scale changes occurred between the two dates. The figures show the classified maps of the considered area obtained by the neural procedure described. A visual inspection suggests that the main large built area has been identified with good accuracy, as well as some specific structures such as the parks inside the city, the Tiber river, the compact old section of the city and the Ciampino airport. In spite of the decametric resolution of the SAR acquisition, several features, even of relatively small dimensions like the trees along the river and the squares with lawns and plants, have been captured.

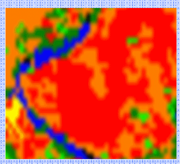

Classification Map of 1999

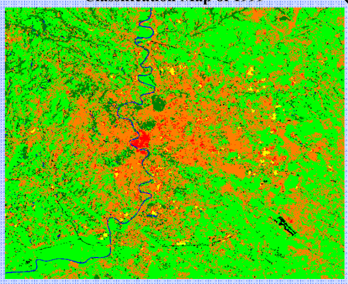

	AS	FO	HD	IB	LD	VE	WS	TOT	Excl Err (%)
AS	189	4	0	0	3	10	2	208	9.13
FO	1	971	0	0	21	18	10	1021	4.90
HD	0	0	232	0	21	1	0	254	8.66
IB	0	0	0	52	0	1	0	53	1.89
LD	3	46	46	0	1974	91	1	2161	8.65
VE	24	72	0	0	154	1391	3	1644	15.39
WS	2	19	0	0	1	4	166	192	[illegible]
TOT	219	1112	278	52	2174	1516	182	5733	
Incl Err (%)	13.70	12.68	16.55	0.00	9.20	8.25	8.79		
Overall Error (%)	[illegible]				k-Coefficient	[illegible]			

URBAN ELECTROMAGNETIC ENVIRONMENT - The complexity of the electromagnetic environment that occurs in urban areas poses severe limitations to the analysis of very-high spatial resolution SAR imagery, since the urban structures are a complex combinations of natural and man-made elements characterized by different materials, shapes, sizes, and orientations. In this second exercise, we want to gain an insight in the field returned by only a single building, since it can derive from several basic contributions from the various parts and structures that compose the whole building. The *first-order* contributions stem from the radar return of elementary scatterers such as the walls of the building, its roof and the terrain which surrounds the structure. The *second-order* contributions generally consider the vertical walls of the structure. In fact, a fraction of the incident field is directly backscattered by the vertical walls, but at the same time, another portion is first scattered by the walls toward the ground and then scattered by the ground to the radar. Also the dual mechanism happens since part of the incident field is scattered from ground in the direction of the vertical walls and then toward the radar. The *third-order* contributions originate only if the ground is rough and concern the reflection from ground to walls to ground and vice-versa.

To analyze such a complex electromagnetic environment, we consider the 14th building of ESA/ESRIN (Frascati, Italy) imaged by the E-SAR in a fully polarimetric mode at L- band. The complex surrounding of the 14th building is analyzed by mean of two perpendicular cuts, orthogonal and parallel to the flight track, respectively, as shown in Figure 2. Considering the orthogonal cut, from right to left (in range direction), we note a first high level signal (pixels 55-57) in correspondence of the parking lots where cars are present. For pixels 53-54, the surface scattering from the road produces a relatively low signal before the high signal from the east side. Pixels 48-52 are the brightest in the image, because of the double bounce reflection mechanism: the typical foreshortening distortion is clearly visible. Pixels within the interval 18-52 are characterized by a rather constant return from the roof, contributed by the surface scattering . At the end of the roof (pixels 9-18) the lower signal corresponds to the shadow of the building and to the asphalted surface. The remaining pixels can be associated with the adjacent building with the same scattering mechanism of pixels 55-57. Considering the parallel cut, the most interesting behaviour is the high level signal of the north and south walls of the building (pixels 3-5 and 11-14): the presence of vertical structures creates a double bounce, thus enhancing the radar return

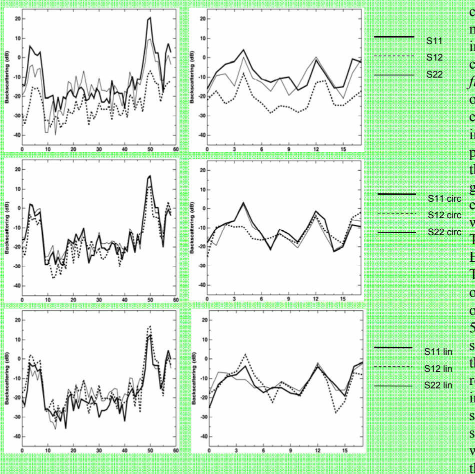

Fig 1. Backscattering course at different polarization of Building 14.

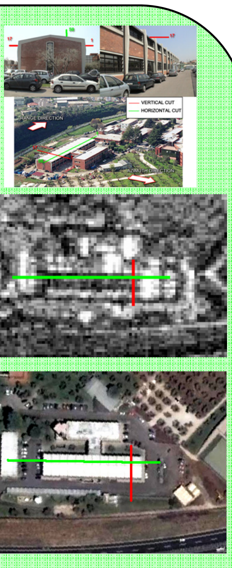

Fig 2. Esrin Building 14 – Aerial view – Radar – Optical Image

CONCLUSIONS – The information contained in multi temporal decametric resolution SAR imagery can be exploited in a relatively straightforward manner for classifying a large urban area, such as the city of Rome.

The very-high resolution polarimetric SAR imagery, on its side, is strongly affected by the complexity and the variety of scattering mechanisms, even for single isolate buildings. For the enhanced resolution, a variety of electromagnetic and geometric effects, which tend to be smeared by a coarser resolution, must be taken into account for a successful *perpixel* classification. Alternative approaches can be devised to better cope with the complex behaviour of very high resolution radar images of man-made objects. As discussed before, the radar signature of a single building is the complex combination of basic scattering mechanisms; all these contributions can be re-assembled and related using an object oriented method, to improve the classification of very-high resolution radar data. This approach is going to be investigated in the near future.